Available online at www.sciencedirect.com

SciVerse ScienceDirect

Ceramics International 39 (2013) 8363–8376

CERAMICS INTERNATIONAL

www.elsevier.com/locate/ceramint

Influence of different additives on the synthesis of VO_2 polymorphs

Yifu Zhang[a], Juecheng Zhang[a,b], Xiongzhi Zhang[a], Yuan Deng[a], Yalan Zhong[a], Chi Huang[a,c,*], Xin Liu[b], Xinghai Liu[d], Shaobo Mo[a,**]

[a]College of Chemistry and Molecular Sciences, Wuhan University, Wuhan 430072, PR China
[b]School of Life Science and Technology, Huazhong University of Science and Technology, Wuhan 430074, PR China
[c]Engineering Research Center of Organosilicon Compound and Material, Ministry of Education of China, Wuhan 430072, PR China
[d]School of Printing and Packaging, Wuhan University, Wuhan 430072, PR China

Received 29 January 2013; received in revised form 6 April 2013; accepted 6 April 2013
Available online 12 April 2013

Abstract

Monoclinic vanadium dioxide VO_2(M) shows a fully reversible first-order metal-to-insulator transition (MIT) with the phase transition temperature (T_c) at about 68 °C. The large-scale and low-cost synthesis of VO_2(M) are a challenge for materials scientists. In this paper, the influence of different additives on the synthesis of VO_2 polymorphs by a hydrothermal route was studied. F, Ti, Cr, Fe, Mo, Sn, Sb and W atoms can promote the formation of VO_2(M), while Mg, Al, Co and Ni atoms are favorable for the synthesis of VO_2(B), whereas, Na, Ca, Mn and Zn atoms have no influence on the formation of VO_2(A). It was found that the T_c of doped VO_2(M) is very sensitive to the doped atoms. Some parameters, such as the temperature, reaction time, initial V_2O_5/oxalic acid molar ratio, tungstic acid concentration, were briefly discussed to give a systematic overview on the synthesis of W-doped VO_2(M). In all cases, the morphologies of the doped VO_2(M) show micro- and nano-rods structures. The T_c of W-doped VO_2(M) can be simply tuned by changing the doping concentration of W atom within appropriate limits. The variable-temperature infrared spectra show that the doped VO_2(M) has outstanding thermochromic characters and optical switching properties. Furthermore, the enlarged-scale experiments for the synthesis of doped VO_2(M) suggest that the same results can be acquired, which makes this route very suitable for practical application.

Keywords: A. Powders: chemical preparation; C. Optical properties; D. Transition metal oxides; D. Vanadium oxides; VO_2(M)

1. Introduction

Low-dimensional materials, including those of zero-dimension, one-dimension (1D), and two-dimensions, have been in the forefront of applied research because they exhibit novel physical and chemical properties, which greatly differ from their bulk counterparts [1–4]. Among them, 1D nanostructures, such as nanotubes, nanobelts, nanorods, and nanowires, are a particularly attractive class of materials because they exhibit lots of novel characteristics owing to their small radial dimen;sion while retaining wire-like connectivity [5]. Moreover, 1D nanostructures have been stimulating significant interest in material chemistry due to their novel chemical and physical properties, which make them have a wide range of potential applications [6–8], including the fabrication of nanoscale electronic, optical, electrochemical, optoelectronic, electromechanical devices, etc. Owing to their special morphology, they can be also used as templates to synthesize some extraordinary materials which can hardly be fabricated by a direct route [3,9–11]. For example, V_2O_3@C core-shell structured nanocomposites can be synthesized using $V_3O_7 \cdot H_2O$@C nanobelts as templates and the as-obtained V_2O_3@C can improve the electrochemical properties of V_2O_3 [3]. Therefore, it is of great interest for materials scientists to fabricate materials with novel structures and morphologies, which may have outstanding properties and applications.

As is well known, vanadium has abundant oxidation states (0–+5), which is usually composed of a variety of binary oxides with the general formula VO_{2+x} ($-0.5 \le x \le 0.5$), such as V_2O_5, V_3O_7, V_4O_9, V_6O_{13}, VO_2, V_2O_3, etc. Over the past decades, numerous efforts have been employed in vanadium

*Corresponding author at: College of Chemistry and Molecular Sciences, Wuhan University, Wuhan 430072, PR China. Tel.: +86 68754224; fax: +86 27 68754067.
**Corresponding author. Tel.: +86 68754224; fax: +86 27 68754067.
E-mail addresses: chihuang@whu.edu.cn, zhyifu123@126.com (C. Huang), sbmo@whu.edu.cn (S. Mo).

0272-8842/$ - see front matter © 2013 Elsevier Ltd and Techna Group S.r.l. All rights reserved.
http://dx.doi.org/10.1016/j.ceramint.2013.04.016

oxides and their derivatives as functional materials because of their layered structures, novel chemical and physical properties [12–23], which make them possess a wide range of promising potential applications, such as cathode materials for reversible lithium batteries, catalysts, gas sensors, intelligent thermochromic windows, laser shield and so on. As a family of vanadium oxides, VO_2 is a representative binary com pound with different polymorphs, including VO_2(B), VO_2(M), VO_2(R), VO_2(A), VO_2(C) [24], recently reported VO_2(D) [25], etc. VO_2(B) with metastable monoclinic structure has attracted interest as a promising cathode material for Li-ion battery, on the basis of not only its proper electrode potential, but also its tunnel structure, through which Li-ions can make intercalation and de-intercalation in reversible Li-ion battery [26]. Besides, VO_2(B) is usually as the precursor to be transformed to VO_2(M/R) [27]. Recently, increasing attention has been paid on tetragonal VO_2(A) (space group: P42/ncm) [28–31], because it shows a metal-semiconductor transition with the phase transition temperature (T_c) at 162 °C, accompanied by a crystallographic transition between a low temperature phase (LTP, P4/ncc, 130 below 162 °C) and a high temperature phase (HTP, I4/m, 87 above 162 °C).

However, among all of VO_2, VO_2(M) is the most important because it shows a fully reversible first-order metal-to-insulator transition (MIT) at a temperature of T_c=~68 °C [32], which is very close to room temperature. VO_2(M), an insulator and IR transparent, monoclinic phase above T_c changes to VO_2(R), a metallic and highly IR reflective, rutile phase [33]. For example, the change in electrical resistivity is in the order of 10^5 below and above T_c. Moreover, the T_c of VO_2(M) can be tuned by doping with W, Mo, Nb, F atoms, etc. or their mixtures [14,34–39]. These features make them have promising applications in smart window coatings for energy-saving and comfort, optical switching devices, Mott field-effect transistors, uncooled IR imaging, laser protection, data storage and so on [14,40–43]. Among of their potential applications, the most important one is “smart window coatings”. The VO_2 material exhibits IR transmission at $T < T_c$, where T is the ambient temperature. However, it becomes IR reflection at $T > T_c$. The above descriptions make it to be required for smart windows. In winter, VO_2 smart window coatings allow infrared solar transmittance and keep the indoor warm. Whereas, in summer, they block infrared solar transmittance and make the indoor cool. If we can make use of VO_2 for the smart windows and in automobiles, electricity consumption can be lowered by 30%, as well as other fuels conserved, because about 50% of the total solar energy is distributed to the infrared spectral range [44–47]. Therefore, VO_2 smart window coatings have been practiced by some researchers [48]. VO_2-based films with high thermochromic quality were deposited by PVD methods in laboratory. However, there are some barriers which restrict the production of these films in low-cost and large-scale. To solve the problem, the route for the synthesis of VO_2/polymer composite films has been proposed. Nowadays, polymer science has been greatly developed. Up to now, highly transparent and durable films are commercially available and a variety of functional fillers have been widely used. While the VO_2 powder is considered as a kind of filler, it can be asserted that all other technical problems have been solved except the availability of high quality filler [42,49,50]. Therefore, the fabrication of low-cost and large-scale VO_2(M) powders is crucial for materials scientists.

So far, various technologies have been developed for producing VO_2(M) powders. These methods generally can be cataloged to reduction of high-valance vanadium oxides [51,52], pyrolysis of vanadium containing precursor [53,54], soft-chemical route [55,56], transforming from VO_2(B) [35,57] or VO_2(A) [43] to VO_2(M) at elevated temperatures, direct confined-space combustion [58], sol–gel synthesis [42] and hydrothermal synthesis [36,37,59–64]. However, most of them are much complex, low efficiency and high cost. Besides, their experimental conditions are very harsh and energy-consuming. Thus, they are not suitable for coating the surface of substrates with a large surface area and industrial applications. On the contrary, in recent years, the hydrothermal synthesis has been paid increasing attention owing to its simple route, low cost, large-scale and mass production.

In 1977, Théobald [62] first reported the synthesis of VO_2 (M) above 350 °C by the hydrothermal reaction in V_2O_3–V_2O_5–H_2O system. Thereafter, there has been few literatures reported on the hydrothermal synthesis of VO_2(M), suggesting the difficulty in obtaining VO_2(M) at low temperature by one step reaction. Up to 2001, Gui et al. [63] mentioned the formation of VO_2(R) by a long-time hydrothermal reduction of NH_4VO_3 by N_2H_4 (at 220 °C for 15 days). But no details about the formed VO_2(R) were given in their paper. Recently, VO_2 (R) hollow spheres with nanorods aggregating on their surface were successfully synthesized by a surfactant-assisted hydrothermal process [61]. Son and his coworkers [59] reported the synthesis of micro- and nano-crystals of VO_2(M) by a hydrothermal method including three steps: (1) V^{4+} solution was obtained by the reaction of V_2O_5, H_2SO_4, and $N_2H_4 \cdot H_2O$; (2) a gray to brown precipitate is formed by adjusting the pH values using NaOH solution; and (3) the above precipitate undergoes hydrothermal treatment at 230 °C for 48 h. Ji et al. [60] directly synthesized VO_2(R) nanorods via the hydrothermal reduction of V_2O_5 by oxalic acid. However, Cao et al. [37], Luisa Whittaker et al. [36] and our groups [29] found that only VO_2(A) can be obtained by the hydrothermal reaction of V_2O_5 and oxalic acid. Cao et al. [37] and Whittaker et al. [36] published that W-doped VO_2(M) snowflakes consisting of nanorods and nanobelts had been synthesized via the hydrothermal reaction of V_2O_5, oxalic acid, and tungstic acid at 240 °C for 7 days and at 250 °C for 48 h, respectively. Our group recently reported the W-doped VO_2(M) nanobelts synthesized using peroxovanadium (V) complexes as the vana dium precursor and ethanol as the reducing agent by a facile one-step hydrothermal approach [65]. However, the influence of different additives on the formation of VO_2 poly;morphs (VO_2(M), VO_2(A) and VO_2(B)) during hydrothermal reaction has not been studied until now, which can guide the large-scale preparation of VO_2(M) for the industrial production.

Herein, we first reported a systematic overview on the synthesis of W-doped VO_2(M) using tungstic acid as the

additive during a hydrothermal approach. Then, the influence of different additives on the formation of VO_2 polymorphs by this hydrothermal route was investigated. Last, the enlarged-scale experiments for the synthesis of doped VO_2(M) were carried out.

2. Experimental section

2.1. Synthesis of W-doped VO_2

All reagents used in the experiments were of analytical grade and used without any further purification. In a typical synthesis, 0.91 g of vanadium pentoxide (V_2O_5), 1.26 g of $H_2C_2O_4 \cdot 2H_2O$ (oxalic acid dihydrate) and an appropriate amount of tungstic acid [n(W)/n(V+W)*100%=0, 0.25%, 0.5%, 0.75%, 1.0%, 1.25%, 1.5%, 2.0%, 3.0%, 4.0% or higher] were dispersed into 40 mL of deionized water with magnetic stirring vigorously for about 10 min at room temperature. After the solution became suspension, the mixed solution was transferred into a 60 mL stainless steel autoclave, which was sealed and maintained at 180–280 °C for 1–96 h and then cooled to room temperature naturally. The products were filtered off, washed with distilled water and absolute ethanol several times to remove any possible residue, and dried in vacuum at 75 °C.

2.2. Synthesis of VO_2 doped with different additives

The synthetic process was the same as Section 2.1, except that the HF, NH_4F, NaOH, MgO, Al_2O_3, $Al(OH)_3$, $Ca(OH)_2$, TiO_2, $Cr(OH)_3$, MnO_2, Fe_2O_3, $Fe(OH)_3$, Co_3O_4, $Ni(OH)_2$, ZnO, molybdenic acid, ammonium molybdate, sodium molybdate, SnO, Sb_2O_3, ammonium tungstate or sodium tungstate took the place of tungstic acid.

2.3. Enlarged-scale experiments for the preparation of doped VO_2(M)

The synthetic process was similar with Section 2.1, except that the quantities of the starting materials were amplified to 20 times in these experiments, which were carried out by a 1.2 L stainless steel autoclave.

2.4. Characterization

The crystalline phases of the as-prepared samples were characterized by X-ray powder diffraction (XRD), preformed on D8 X-ray diffractometer equipment with Cu $K\alpha$ radiation, λ=1.54060 Å. The patterns were recorded over the angular range 8–80° (2θ) with a scan speed of 4°/min. The narrow XRD patterns were collected with 2θ ranging from 26° to 29° with a scan speed of 0.2 deg/min. The chemical composition of the samples was confirmed by the means of the energy dispersive X-ray spectrometer (EDS) attached to a scanning electron microscope (SEM, Quanta 200), X-ray photoelectron spectroscopy (XPS, KRATOS, XSAM800 with MgKα 1253.6 eV 16 mA × 12 kV) and X-ray fluorescence (XRF, XRF-1800, Shimadzu, Japan). The morphology of the products was observed by SEM (Quanta 200) operated at 30 kV. The phase transition temperature (T_c) of the samples was measured by differential scanning calorimetry (DSC, DSC822^e, METTLER TOLEDO) in a heating rate at 5 °C/min with a liquid nitrogen cooling system. Optical properties of the samples were tested by variable-temperature Fourier transform infrared spectroscopy (FT-IR, NICOLET 5700) with an adapted heating controlled cell. FT-IR patterns of the solid samples were measured using KBr pellet technique from 4000 to 400 cm^{-1} with a resolution of 4 cm^{-1}. About 1 wt% of the samples and 99 wt% of KBr were mixed homogeneously, and then the mixture was pressed to a pellet.

3. Results and discussion

3.1. Characterization of W-doped VO_2(M)

3.1.1. XRD diffraction patterns

In this section, unless otherwise stated, the following experiments were carried out using tungstic acid as the additive. Fig. 1 shows the XRD patterns of W-doped VO_2 prepared at different temperatures for 48 h using 0.91 g of V_2O_5, 1.26 g of $H_2C_2O_4 \cdot 2H_2O$ and 1.0 at% of tungstic acid. The products obtained at 180 and 210 °C can be indexed to the metastable VO_2(B) polymorph (JCPDS, no. 31-1438) [66], which has attracted increasing interest as a cathode material for Li-ion batteries. Upon increasing the temperature of the hydrothermal reaction to 230 °C, the isolated products appear to be a mix of the original VO_2(B) along with a significant proportion of the monoclinic VO_2(M) polymorph (JCPDS, no. 43-1051) [67], as depicted in Fig. 1c. However, VO_2(M) was obtained when the reaction temperature was above 280 °C. The as-obtained

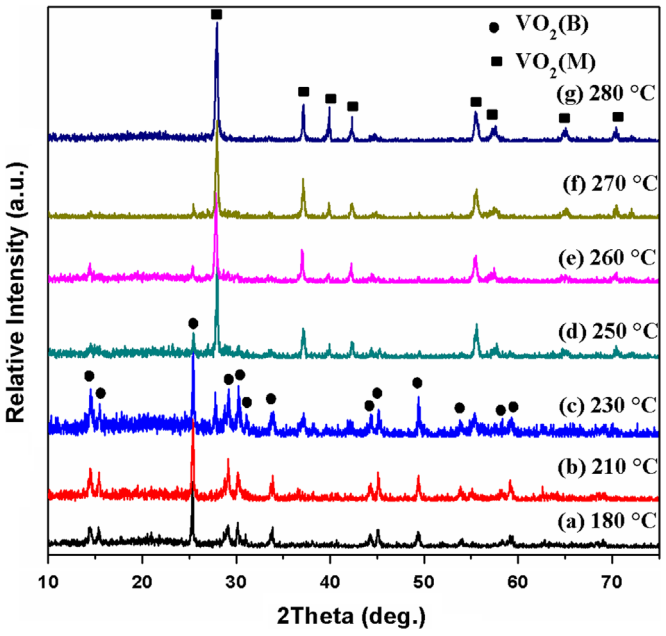

Fig. 1. XRD patterns of W-doped VO_2 prepared at different temperatures.

VO_2(M) is phase pure and exclusively monoclinic in crystal structure within the detection limits of powder XRD. Therefore, the transformation of crystal phases from VO_2(B) to VO_2(M) in our hydrothermal system takes place between 230 and 280 °C, which is much lower than the reference's value [62]. This phenomenon reveals VO_2(M) can be formed at a comparatively low temperature in the presence of H_2WO_4, which greatly reduces the cost and technique of its industrial production.

Fig. 2 represents the XRD patterns of W-doped VO_2 synthesized by the hydrothermal treatment at 280 °C for different reaction times (0.91 g of V_2O_5, 1.26 g of $H_2C_2O_4 \cdot 2H_2O$ and 1.0 at% of tungstic acid). The diffraction patterns in this panel illustrate that after shorter reaction times, such as 1, 3 and 6 h, a residual amount of metastable VO_2(B) remains in the isolated products. Upon further increasing the reaction time to 12 h or longer, the products appear to be exclusively phase-pure VO_2(M), suggesting that the metastable VO_2(B) phase is an inter mediate for the synthesis of VO_2(M) structures. It can be observed from Fig. 2, that the transformation from VO_2(B) to VO_2(M) is very short compared with the previous [36,37].

The initial V_2O_5/oxalic acid molar ratio plays a significant role in synthesizing high purity W-doped VO_2(M). Fig. 3 shows the XRD patterns of the products synthesized with different V_2O_5/oxalic acid molar ratios (0.91 g of V_2O_5, 1.0% of tungstic acid and at 280 °C for 48 h). As depicted in Fig. 3, the preparation of phase-pure VO_2(M) is achieved only within a limited molar ratio window (V_2O_5/oxalic acid = 1/2–1/3), whereas various mixed VO_x phases are observed below and above this optimum range of molar ratio. In this context, binary vanadium oxides are known to have an incredibly rich phase diagram because of the diversity of vanadium oxidation states (0–+5), local coordination environments (square pyramidal, tetrahedral, octahedral, and trigonal bipyramidal), and

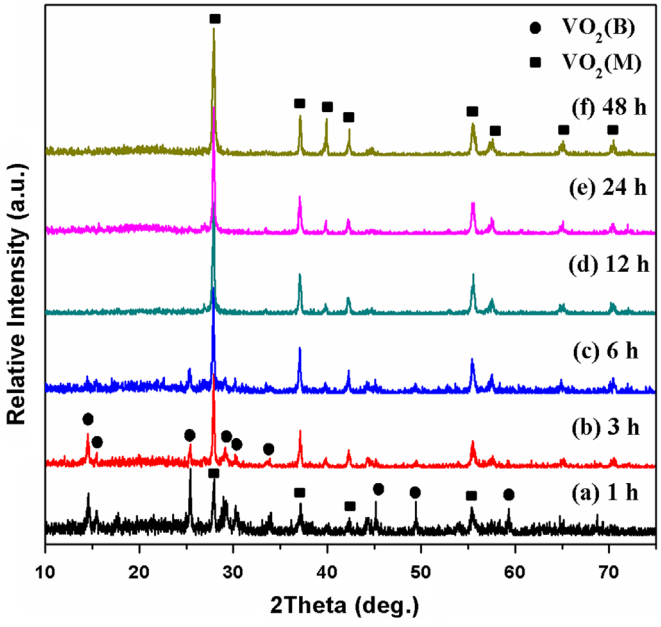

Fig. 2. XRD patterns of W-doped VO_2 synthesized at 280 °C for different periods of reaction time.

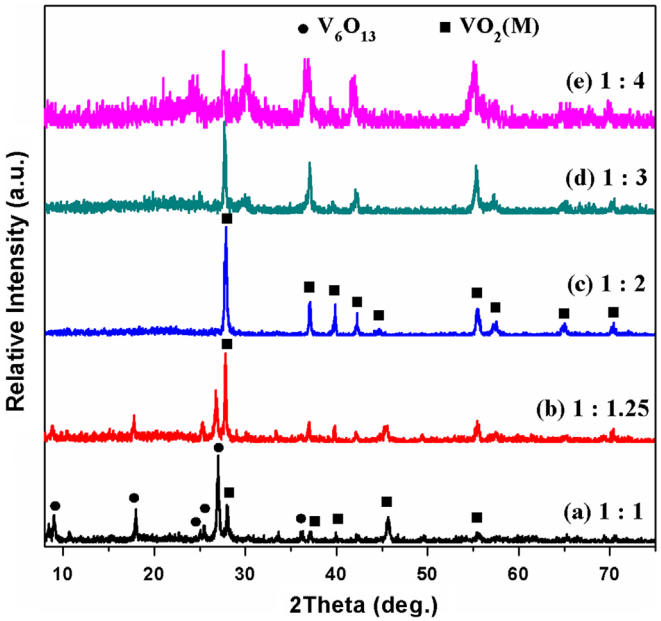

Fig. 3. XRD patterns of the products synthesized with different mol ratios of $V_2O_5/H_2C_2O_4 \cdot 2H_2O$.

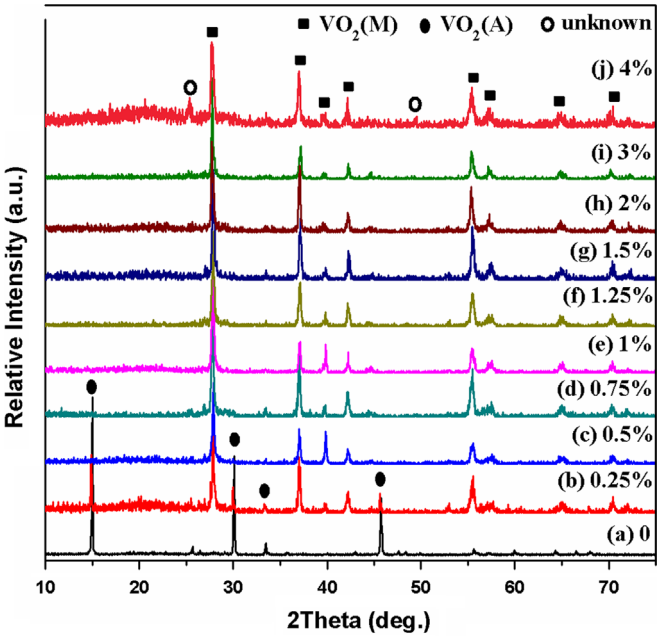

Fig. 4. XRD patterns of the as-obtained VO_2 with various extents of W doping.

their ability to accommodate point defects through crystallographic shear [36,68]. Thus, it is imperative to maintain an appropriate concentration of the reducing agent to achieve the correct stoichiometry in the reduction of V_2O_5 to successfully form rutile phase of VO_2.

The XRD patterns of undoped and W-doped VO_2 with various extents of W doping are shown in Fig. 4. Only VO_2(A) can be obtained from Fig. 4a, revealing VO_2(M) cannot be stabilized under the hydrothermal conditions in the absence of W doping, in agreement with the literatures [29,36,37].

VO_2(M) can be detected with 0.25 at% of W doping. Consequently, phase-pure monoclinic W-doped VO_2(M) are obtained for W-doping greater than 0.50 at% by this hydrothermal approach. At the relatively low doping concentrations studied here (0.5–3.0 at%), no segregated WO_x phases have been detected by XRD, suggesting that the W atoms enter into the crystal lattice of VO_2 matrix and the homogeneous solid-solutions of $W_xV_{1-x}O_2$(M) are formed. However, when the concentration of W-doped fractions is increased to 4.0 at% or higher, some unknown peaks are observed due to the residual dopants in the system, as shown in Fig. 4j. The reported W doping of the sublattice here is based on W atom concentration added to the initial reaction, as shown in Section 2.1.

To further reveal whether W atoms were doped into the VO_2(M) lattice, the narrow XRD patterns of W-doped VO_2(M) with various extents of W doping were carried out, as shown in Fig. 5, where 2θ is ranging from 26° to 29° with a scan speed of 0.2 deg/min. With the increasing of W doping, the most prominent reflection, which is indexed to the (011) plane of VO_2(M), shows a shift toward smaller 2θ. This means that the adjacent interplanar spacing d_{011} increases with increasing extent of substitutional W incorporation within the VO_2(M) lattice, which is consistent with the larger atomic radius of W. For example, the *d*-spacing increases from 3.207 Å for undoped VO_2(M) (JCPDS, no. 43-1051) to 3.221 Å for 1.0 at% W doping into the vanadium sublattice. These results indicate that W atoms substitute V atoms in VO_2 lattice.

To verify if other tungstates can get the similar results, the ammonium tungstate and sodium tungstate were used as the additives to do the experiments and their corresponding XRD patterns were depicted in the Supplementary data (Figs. S1 and S2), which indicated that W-doped VO_2(M) were also obtained.

3.1.2. EDS, XPS and XRF analysis

Based on the above XRD results, the tungstates can promote the formation of VO_2(M) by the hydrothermal reduction of V_2O_5 by $H_2C_2O_4$. When the reaction conditions are appropriately controlled, there are no impure phases detected by XRD, which suggests the formation of homogeneous $W_xV_{1-x}O_2$(M) solid solutions. To further reveal whether W atoms are doped into the VO_2(M) lattice, some corresponding tests, including EDS, XPS, and XRF, were carried out.

The composition of the as-obtained W-doped VO_2(M) was investigated by EDS and XPS. Fig. 6 shows a typical EDS spectrum of W-doped VO_2(M) sample (2.0 at%), which reveals that the sample only consists of O, V and W elements. Fig. 7 represents the typical XPS spectra of W-doped VO_2(M) sample (2.0 at%), which contains four elements: O, V, W and C, where the C is attributed to surface contamination (Fig. 7a). The O_{1s} peak is centered at its standard value (530.0 eV) and $V_{2p3/2}$ is centered at 516.8 eV, as depicted in Fig. 7b and c, respectively. The value of $V_{2p3/2}$ peak is slightly higher than that of pure VO_2 powder [69,70], but it is in agreement with the reports of W-doped VO_2(M) [42], suggesting that the binding energy of $V_{2p3/2}$ increased slightly after W doping. The peaks located at 245.8 (Fig. 7a), 37.4 and 35.3 eV (Fig. 7d) are attributed to W_{4d}, $W_{4f5/2}$ and $W_{4f7/2}$, respectively, indicating the successful synthesis of W-doped VO_2. According to the standard binding energy, the existing form of tungsten ion in these powders is W^{6+} [54,70]. Besides, the binding energy centered at 42.3 eV in Fig. 7d is indexed to V_{3p}.

The variation of the final content for different elements mainly depends on the solubility of different chemicals under the hydrothermal condition. To determine the final doping amount of W in the samples, XRF was performed. Fig. 8 shows the W atomic percent in W-doped VO_2(M) as a function of W atomic percent in feed, which reveals that the real contents of W in final products are slightly higher than its corresponding nominal contents. These results indicate that some vanadium remains in the solution after hydrothermal treatment, which is consistent with the reference [42]. However, the

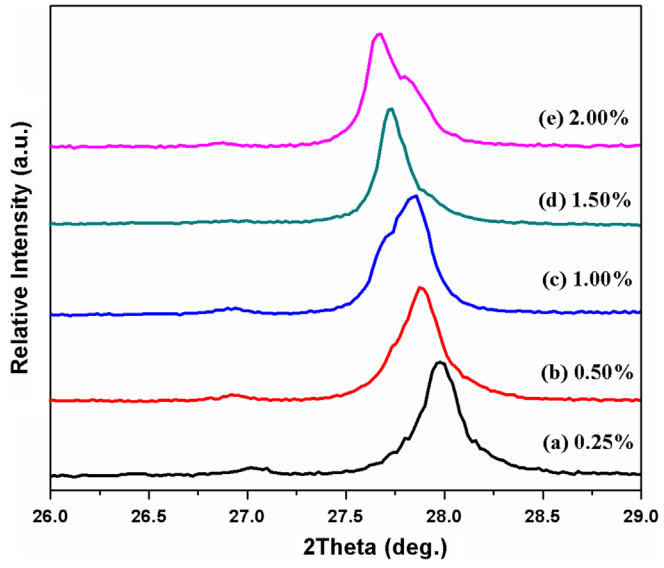

Fig. 5. Narrow XRD patterns ($26° \le 2\theta \le 29°$) of VO_2(M) with various extents of W doping.

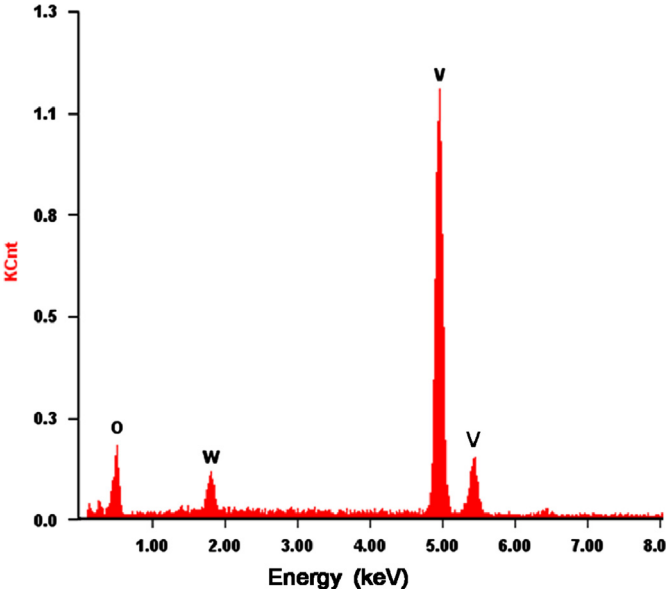

Fig. 6. Typical EDS spectrum of W-doped VO_2(M).

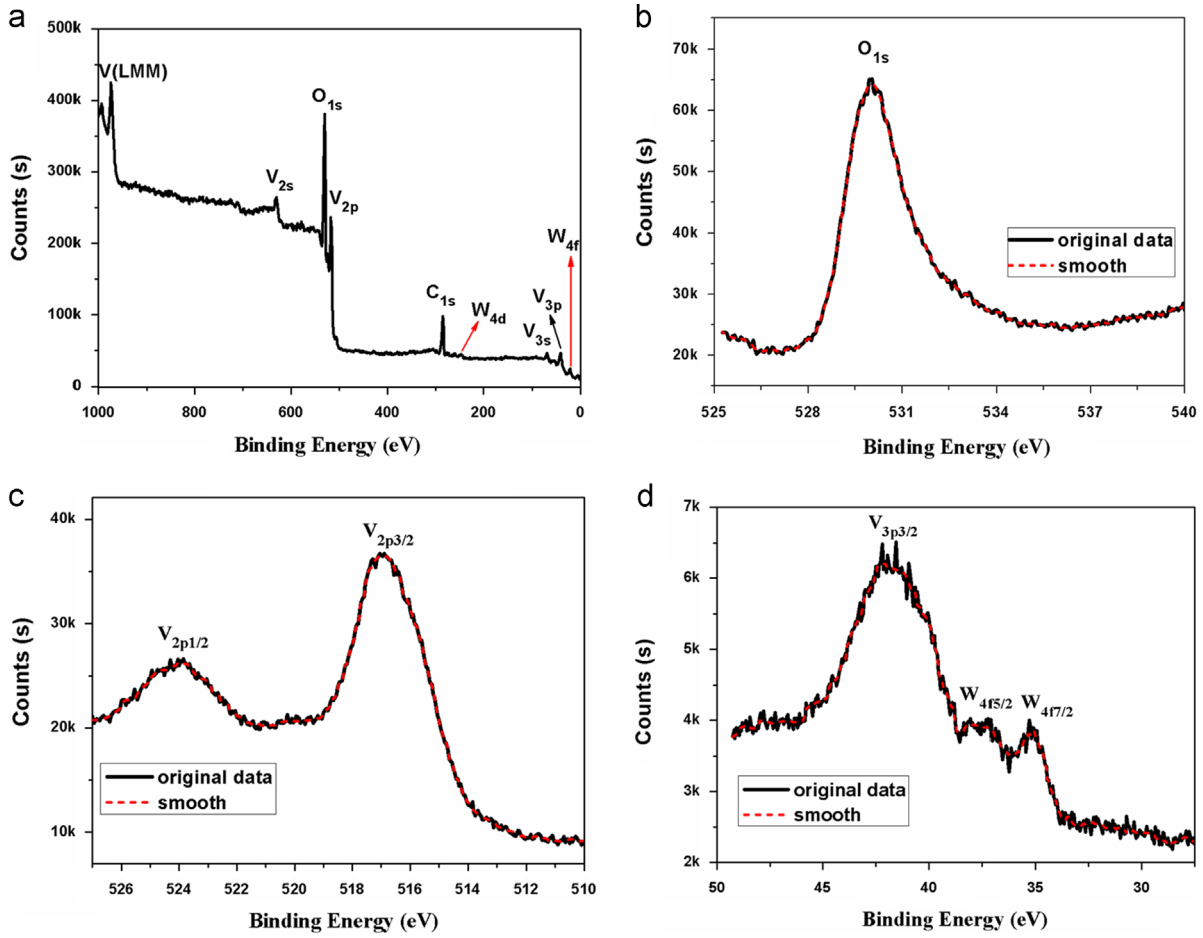

Fig. 7. Typical XPS spectra of W-doped VO_2(M): (a) survey spectrum; (b) core-level spectrum of O_{1s}; (c) core-level spectrum of V_{2p}; and (d) core-level spectrum of W_{4f}.

tungsten atomic percent in $W_xV_{1-x}O_2$(M) solid solution is basically the same as the W atomic percent in feed, indicating that the tungsten content in $W_xV_{1-x}O_2$(M) solid solution can be easily controlled by the change of dopants concentration in our process, which is crucial for the large-scale manufacture.

3.1.3. DSC analysis

W is the most effective dopant for reducing the T_c on per atomic percent basis. Here, the phase transition properties of W-doped VO_2(M) were studied by DSC. Fig. 9 shows DSC data demonstrating the influence of W doping on the T_c and hysteresis of the MIT. As noted above, polycrystalline VO_2(M) exhibits a reversible thermally induced first-order MIT at 68 °C, between a high temperature metallic phase and a low temperature insulating phase. The phase transition is first-order in nature and thus associated with a latent heat and a pronounced change in the specific heat capacity [36,43]. The two primary contributions to the latent heat at the phase transition arise from the lattice distortion and the entropy change for conduction electrons because of the discontinuity in the carrier density. Fig. 9a shows the representative DSC curves of W-doped VO_2(M) (1 at% of W), which display sharp endothermic and exothermic profiles upon heating and cooling cycles, respectively. The T_c is about 53 °C in the heating cycle and 44 °C in the cooling cycle, which is due to the hysteresis behavior. Fig. 9b summarizes the T_c associated with the insulator→metal and metal→insulator phase transitions as a

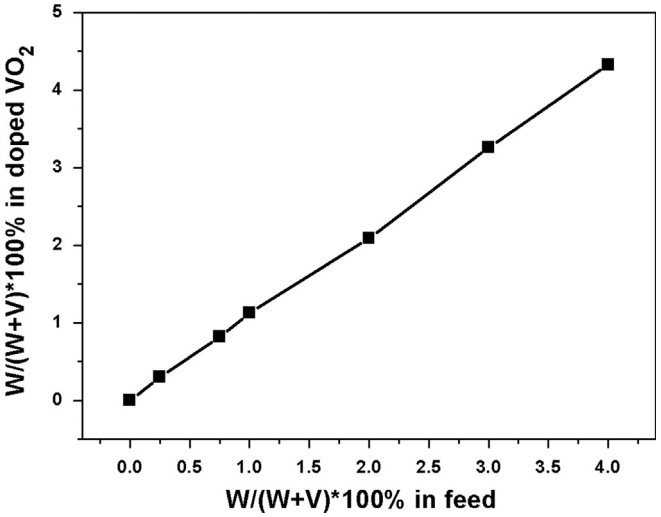

Fig. 8. Relationship of the W atomic percent in W-doped VO_2(M) solid solution and W atomic percent in feed.

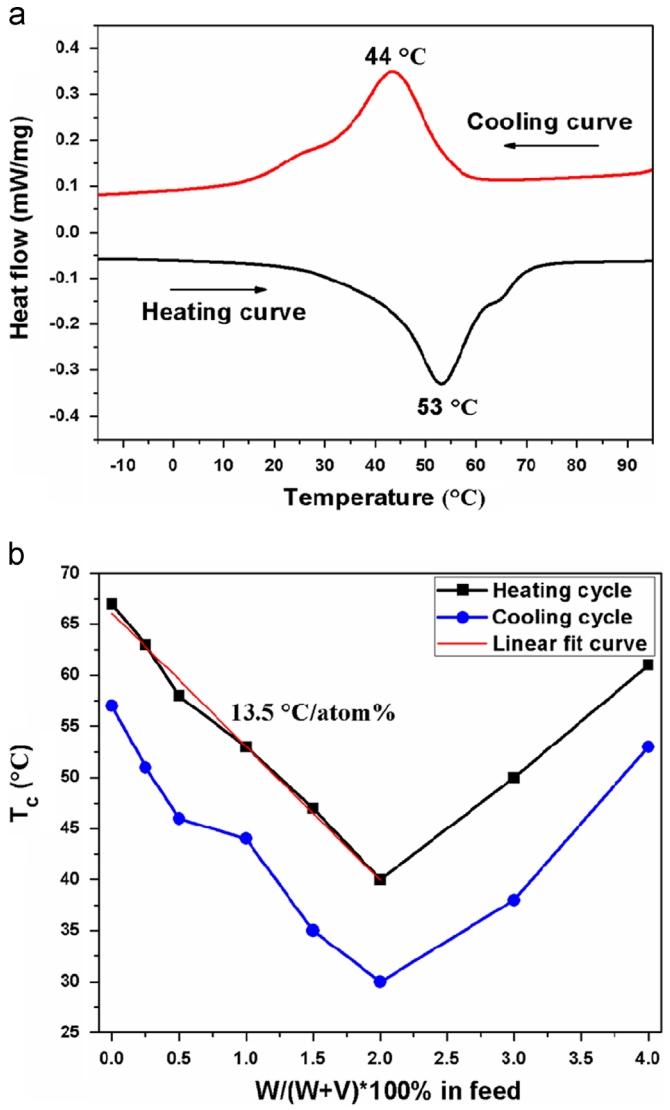

Fig. 9. Effect of W doping on the phase transition temperature (T_c): (a) the typical DSC curves for W-doped VO_2(M) with 1.0 at% upon heating and cooling cycles; and (b) relationship between T_c and W contents.

function of the extent of W doping. When the concentration of tungsten is not larger than 2.0 at%, the T_c of W-doped VO_2(M) is decreased with the increase of tungsten concentration, revealing that W atoms can be effectively doped into VO_2(M) and the T_c of $W_xV_{1-x}O_2$(M) can be easily tuned. There is an almost linear dependence of the T_c on the concentration of tungsten not larger than 2.0 at%, for both the heating and cooling cycles, and the least square approximation gives a T_c reduction efficiency of 13.5 °C/at% W. However, further doping with W has a negative influence on T_c, because the doping atoms cannot be effectively doped into VO_2(M) lattice with the higher concentration of dopants. The phase transition behavior of the W-doped VO_2(M) here differs in some important respects from previous observations of W-doped VO_2(M) powders, thin films, and single crystals [71,72]. First, a very pronounced hysteresis is observed between the insulator→metal and metal→insulator transitions. Second, the insulator→metal and metal→insulator transitions show dramatically different dependences on the extent of substitutional W doping. Third, the T_c for both transitions initially follows a quasi-linear dependence but subsequently rises with W doping exceeding 2.0 at%.

3.1.4. SEM analysis

The morphology and size of the typical samples were investigated by SEM. Fig. 10 depicts the representative morphologies of W-doped VO_2(M) prepared by this hydrothermal reduction. It can be observed that the W-doped VO_2(M) predominantly consists of a large quantity of uniform micro- and nano-structures with well-defined facets. The diameter of rod-like structures ranges from 100 to 500 nm, and the length is up to several tens of micrometers, which leads to the formation of rods with an ultrahigh-aspect-ratio. As suggested by the XRD patterns in Figs. 1–4, while mapping the multi-dimensional parameter space, the reaction temperature, reaction time, initial V_2O_5/oxalic acid molar ratio and W doping concentration exert distinctive influences on the morphologies and crystal structures of the products. Figs. S3, Fig. S4, Fig. S5 and Fig. S6 (Supplementary data) illustrate the influence of the reaction temperature, reaction time, $V_2O_5/H_2C_2O_4 \cdot 2H_2O$ ratio and contents of W doping on the morphologies of the obtained products. All the SEM images show the as-obtained samples have rod-like morphology.

3.1.5. Optical properties

The "smart window coating" is the most important application of VO_2(M). In this paper, the optical properties of W-doped VO_2(M) (1.0 at%) were investigated by variable-temperature infrared spectra of the heating and cooling cycles, as depicted in Fig. 11. Fig. 11a describes the process of the phase transition of VO_2(M) below and above T_c, indicating its T_c is at 54 °C in the heating cycles and at 42 °C in the cooling cycles, which agrees with the results of DSC (Fig. 9). As shown in Fig. 11b, a significant change in optical properties on switching is observed based on different IR transmittances below or above T_c. At 80 °C, the sample exhibits low transmittance in IR spectra, however, the sample exhibits high trans mittance at 25 °C. The difference in transmittance suggests that the as-obtained W-doped VO_2(M) has good thermochromic property. Two spectra below T_c in Fig. 11b almost have the same optical transmission, indicating the good reversibility of the sample. Besides, the heating and cooling curves in Fig. 11 are asymmetric due to the hysteresis behavior in the sample.

3.2. The influence of different additives on the formation of VO_2 polymorphs

As suggested by the W-doped VO_2(M) discussed above, W^{6+} ions in the system can stabilize the phase and structure of VO_2(M), which stimulates us to study other additives influenced on the synthesis of VO_2 by this hydrothermal reaction. Thus, a serial of experiments using different additives as the doping reagents were carried out and their corresponding results were summarized in Table 1. It can be seen from

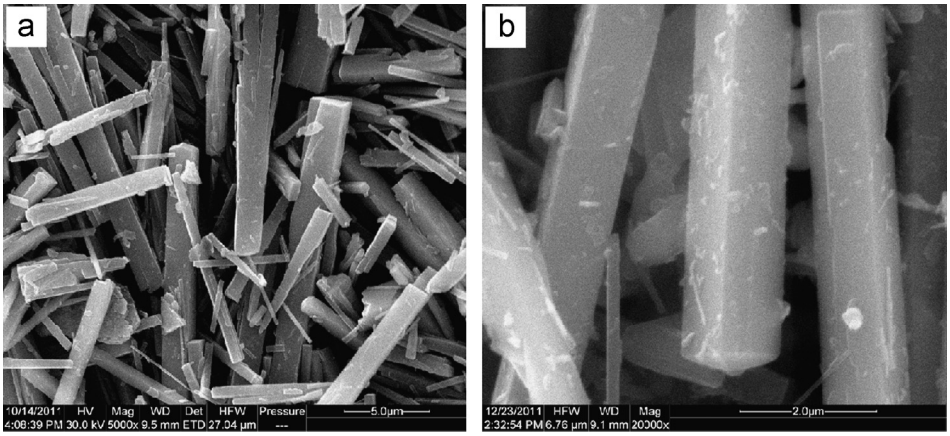

Fig. 10. Typical SEM images of W-doped VO_2(M): (a) a lower magnification; and (b) a higher magnification.

Table 1, that F, Ti, Cr, Fe, Mo, Sn, Sb and W are favorable for the formation of VO_2(M), while Mg, Al, Co and Ni facilitate the synthesis of VO_2(B), whereas, only VO_2(A) is obtained with the atoms Na, Ca, Mn or Zn, which indicates that these additives have no influence on the synthetic process of VO_2(A) compared with the results without the presence of additives (Fig. 4a).

Through the above experimental results, we know that the additives are crucial for the synthesis of VO_2(M). Although the detailed formation mechanism of VO_2(M) by the hydrothermal reduction of V_2O_5 by $H_2C_2O_4$ in the presence of additives is not entirely clear, we presume it can be attributed to the assistant function of the additives. In order to understand the effects of the additives on the phase transformation mechanism, we first have to know the phase transition among VO_2(B), VO_2(A), and VO_2(M). In the recent reports [29,36,37,73–75], VO_2(M/R) cannot be directly synthesized under the hydrothermal conditions in the absence of additives at the temperatures ranging from 180 to 300 °C. Instead of VO_2(M/R), only VO_2(B) and VO_2(A) can be prepared. Théobald [62] studied the phase transformation $VO_2(B) \rightarrow VO_2(A) \rightarrow VO_2(M)$ by the hydrothermal reaction of the V_2O_3–V_2O_5–H_2O system, and it was found that VO_2(B), VO_2(A), and VO_2(M) could be formed at 180, 220 and 350 °C, respectively. Oka et al. [76] reported only VO_2(A) could be achieved via the hydrothermal method. On the basis of the experiments of Théobald and Oka, Galy [77] proposed that the phase transition $VO_2(B) \rightarrow VO_2(A)$ is simply a crystallographic slip $Cs = 1/3[-100](001)$, occurring in the median plane of the double layers assembled by VO_6 octahedra of the VO_2(B) [37]. The mechanochemical activation broke the weakest bonds of the structure and promoted a simple cooperative displacement to give the VO_2(A). Meanwhile, Leroux studied the phase transformation $VO_2(B) \rightarrow VO_2(M)$ *in situ* by electron microscopy [78]. The long range order of the VO_6 octahedra was mostly destroyed with increasing temperature, leading to a breakage of the interconnections between different octahedras, which were either corner sharing or edge sharing in the VO_2(B) structure. Upon continuing heating, the platelets assembled by VO_6 octahedra abruptly broke up into nano-crystallites and half of the VO_6 octahedra re-oriented to form the rutile structure. Such breaking up is clearly necessary due to the completely different arrangement of the VO_6 octahedra in both structures. Although VO_2(M) is more energetically stable than VO_2(A), the breaking of the interconnections between different octahedra needs more energy than the crystallographic slip. Consequently, VO_2(B) transforms into VO_2(A) and then VO_2(M) under hydrothermal conditions. In the doped VO_2(M), the substitution of a part of V atoms with Ti, Cr, Fe, Mo, Sn, Sb or W atoms can induce the distortion of the VO_6 octahedra, making the breaking of the interconnections between different octahedras easier than the crystallographic slip. Besides, the substitution of a part of O atoms with F atoms can also obtain the same results. F-doped VO_2(M), which has not been synthesized by the hydrothermal route in the reports, shows a new idea to synthesize doped VO_2(M) by the substitution of O^{2-} with anions. Whereas, the VO_6 octahedra can be stabilized in the presence of Mg, Al, Co or Ni atoms, resulting in the formation of VO_2(B). However, Na, Ca, Mn or Zn atoms have no influence on the synthesis of VO_2(A). There may be two reasons: (1) these atoms have little effect on the distortion of the VO_6 octahedra; and (2) Na^+ dissolved in the solution can seldom take part in the reaction, while $M_2C_2O_4$ (M = Ca, Mn or Zn) as the insoluble salts are very stable under this hydrothermal route (Supplementary data), so they cannot participate in the reaction, either. Therefore, the synthesis of VO_2(M), VO_2(A) or VO_2(B) by the hydrothermal reaction can be easily controlled by adjusting the additives, which can guide the large-scale preparation of VO_2(M) for the industrial production.

Fig. 12 depicts the morphologies of doped VO_2(M) with different additives. In all cases, we note the formation of highly faceted micro- and nano-rods structures wherein the lengths exceed the diameters, in agreement with the SEM observations of W-doped VO_2(M) discussed above. The micro and nano-rods are expected to result from the intercalation of reducing agents between the layers of V_2O_5, followed by lattice expansion, cleavage, and exfoliation of stacks of V_2O_5 sheets [36,73].

As suggested by the XRD patterns in Fig. 2 and SEM images in Fig. S4, we know that VO_2(B) is the intermediate product to synthesize doped VO_2(M). After 1 or 3 h, VO_2(B)

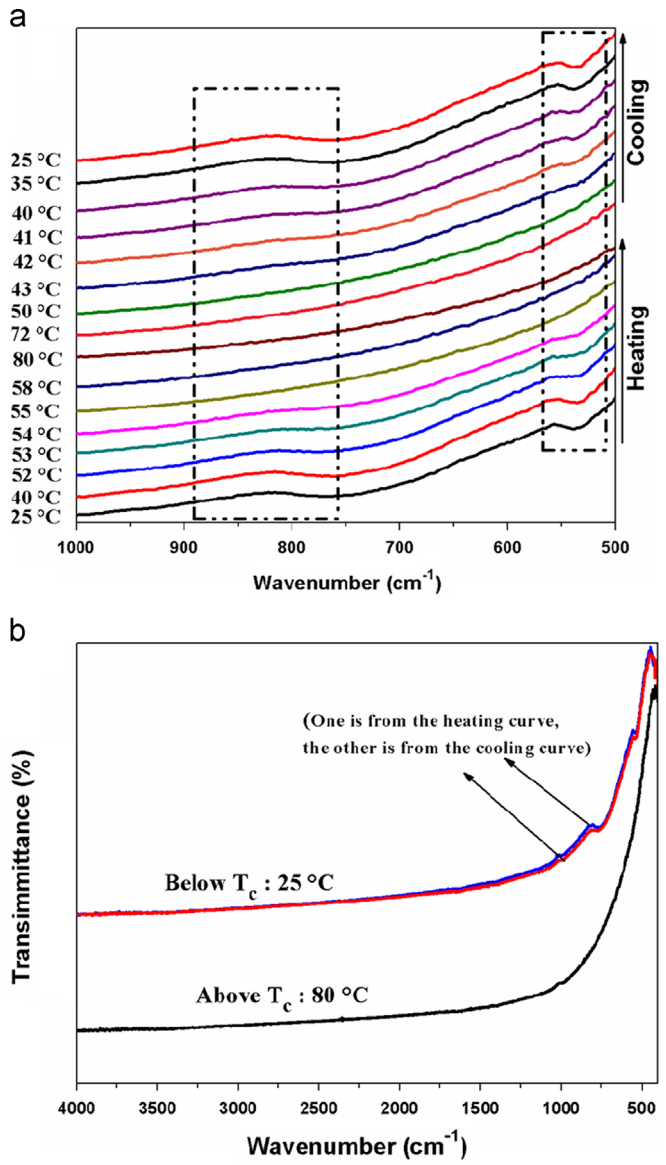

Fig. 11. The variable-temperature IR of 1.0 at% W-doped VO_2(M): (a) IR curves with different temperatures; and (b) IR curves below and above T_c.

nanorods are formed, and then VO_2(B) nanorods are converted to doped VO_2(M) nanorods with prolonging the time, in the case of the phase transformation $VO_2(B) \rightarrow VO_2(A)$ reported previously [29,30]. The basic reaction we employed for the syn thesis of VO_2 in our hydrothermal synthesis can be formulated in the following equation:

$$V_2O_5+2H_2C_2O_4 \rightarrow 2VO_2+3CO_2+CO+2H_2O$$

Although the exact growth mechanism of VO_2(M) micro- and nano-rods is not clear at the current stage, a possible growth mechanism is proposed as the "Reaction–Transformation–Dissolution–Recrystallization" (RTDR) mechanism, which mainly contains four steps as follows: (1) VO_2(B) nanorods are fast formed by the hydrothermal reaction between V_2O_5 and $H_2C_2O_4$ in the presence of additives, as shown in Fig. 2a and Fig. S4a. (2) VO_2(B) is transformed to VO_2(M), as depicted in Fig. 2b, c and Fig. S4b. (3) The irregular and broken fragments of VO_2(M) is dissolved into the solution to help the growth of VO_2(M) nanorods, which can be observed from Fig. S4b–d. (4) VO_2(M) nanorods are continuing to grow and the fragments become fewer and fewer. In a word, the formation of VO_2(M) micro- and nano-rods can be described as the process of transformation, dissolution and recrystallization [29].

Table 1
The influence of different additives on the phase of the products.

No.[a]	Additives	Doped atoms	Phases[b]	VO_2(M) (%)[c]
1	–	–	VO_2(A)	0
2	HF	F	VO_2(M), VO_2(A)	64
3	NH_4F	F	VO_2(A), VO_2(M)	34
4	NaOH	Na	VO_2(A)	0
5	MgO	Mg	VO_2(B)	0
6	Al_2O_3	Al	VO_2(A), VO_2(B)	0
7	$Al(OH)_3$	Al	VO_2(A), VO_2(B)	0
8	$Ca(OH)_2$	Ca	VO_2(A)	0
9	TiO_2	Ti	VO_2(A), VO_2(M)	47
10	$Cr(OH)_3$	Cr	VO_2(A), VO_2(M)	37
11	MnO_2	Mn	VO_2(A)	0
12	Fe_2O_3	Fe	VO_2(A), VO_2(M)	16
13	$Fe(OH)_3$	Fe	VO_2(M), VO_2(A)	71
14	Co_3O_4	Co	Major VO_2(A), minor VO_2(B)	0
15	$Ni(OH)_2$	Ni	VO_2(B)	0
16	ZnO	Zn	VO_2(A)	0
17	Molybdenic acid	Mo	VO_2(M)	100
18	Ammonium molybdate	Mo	VO_2(M)	100
19	Sodium molybdate	Mo	VO_2(M)	100
20	SnO	Sn	VO_2(A), VO_2(M)	46
21	Sb_2O_3	Sb	VO_2(A), VO_2(M)	27
22	tungstic acid	W	VO_2(M)	100
23	Ammonium tungstate	W	VO_2(M)	100
24	Sodium tungstate	W	VO_2(M)	100

[a]Reaction conditions: 0.91 g of V_2O_5 powder, 1.26 g of $H_2C_2O_4 \cdot 2H_2O$, 40 mL of H_2O, 1.0 at% of the additive atoms and the reaction temperature and time are at 280 °C for 48 h.
[b]The phases of the products were examined by XRD.
[c]Percentage of VO_2(M) among the total product calculated by comparing the intensity of the strongest XRD lines with that of VO_2(A) and VO_2(B).

Table 2 summarizes the influence of different doped atoms on the T_c of the doped VO_2(M). The T_c of the samples is decreased to 53, 56 and 53 °C with the doped W, Mo and F atoms, respectively, which suggests that W, Mo and F atoms can reduce the T_c, in agreement with the previous reports [14,34–38]. However, the Ti, Cr, Fe, Sn and Sb atoms which can promote the formation of VO_2(M) have little effect on the T_c. Up to now, the research about the exact mechanism how the doped atoms can reduce the T_c of VO_2(M) is still processing [79]. Some scientists have tried to disclose the reduction mechanism taking W atom as an example. According to the model of Tang et al. [71], W^{6+} penetrates into the crystal lattice of VO_2 and substitutes the V^{4+} ion. As a result of charge compensation, V^{3+}–V^{4+} and V^{3+}–W^{6+} pairs along the

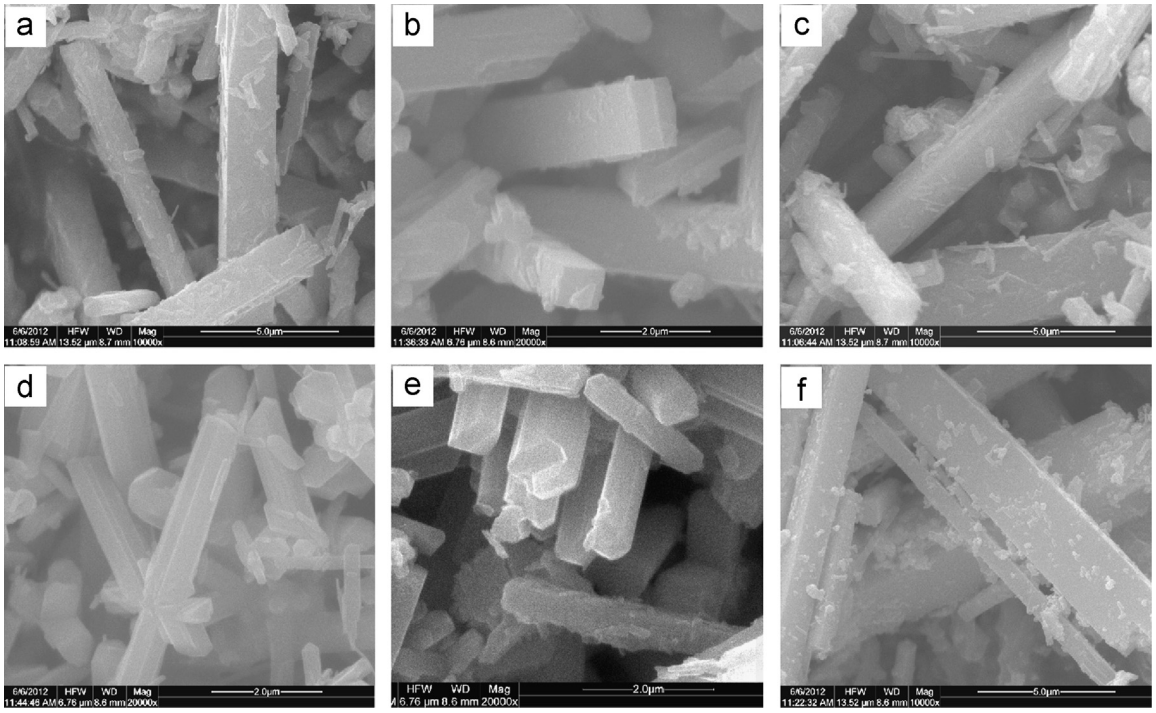

Fig. 12. SEM images of doped VO_2(M) solid solution with different dopants: (a) F; (b) Ti; (c) Cr; (d) Fe; (e) Mo; and (f) Sb.

Table 2
The results of the DSC for samples doped with different elements.

No.	Doped atom (1.0 at%)	T_c (heating curve)/°C	T_c (heating curve)/°C
1	F	53	43
2	Ti	67	53
3	Cr	68	52
4	Fe	66	48
5	Mo	56	53
6	Sn	68	54
7	Sb	67	56
8	W	53	44

a-axis of the monoclinic VO_2 cell are formed. With the enhancement of the electron concentration from the presence of W donors, the loss of V^{4+}–V^{4+} pairs becomes more and more obvious, resulting that the semiconductor phase becomes destabilized and the band gap is reduced. Thus, the metal-to-semiconductor transition temperature is decreased. Based on the above results, the research about mechanism of reducing the T_c of VO_2(M) by doping still requires a lot of effort by scientists.

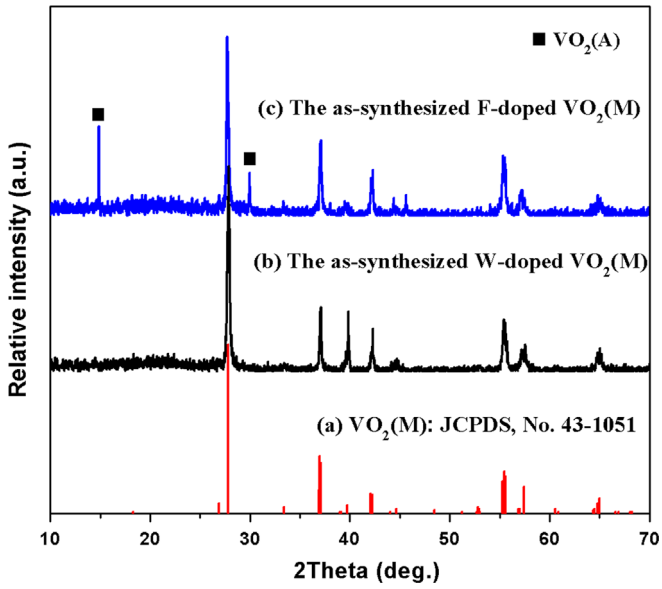

Fig. 13. XRD patterns of W- and F-doped VO_2(M) prepared by the enlarged-scale experiments.

3.3. The enlarged-scale experiments for preparing doped VO_2(M)

So far, many methods have been developed for the synthesis of VO_2(M) and doped VO_2(M). However, there are few literatures reported the large-scale and facile synthesis of VO_2(M) and doped VO_2(M). In this paper, we amplify the experiments to 20 times, which is very meaningful before their enlarged-scale experiments. Excitingly, the similar results were obtained based on the observation of XRD (Fig. 13), SEM (Fig. 14) and DSC (Fig. 15), the suggestive of its potentially industrial production in future. As shown in Fig. 13, W- and F-doped VO_2(M) can be successfully synthesized by this pilot-scale experiments. The SEM images (Fig. 14) reveal that the as-obtained products consist of highly faceted micro- and nano-belts structures with rectangular cross-sections. The T_c of W-doped VO_2(M) is about 53 °C in the heating cycle and 46 °C in the cooling cycle, while the T_c of F-doped VO_2(M) is

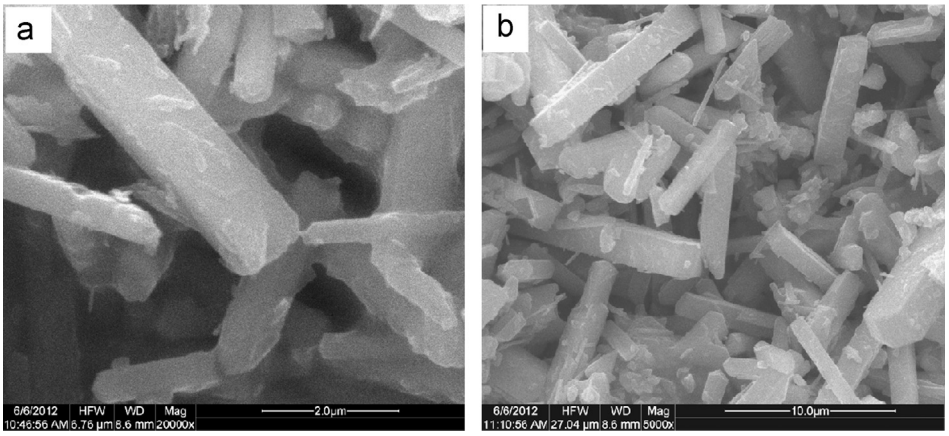

Fig. 14. SEM images of W- and F-doped VO_2(M) prepared by the enlarged-scale experiments: (a) W-doped; and (b) F-doped.

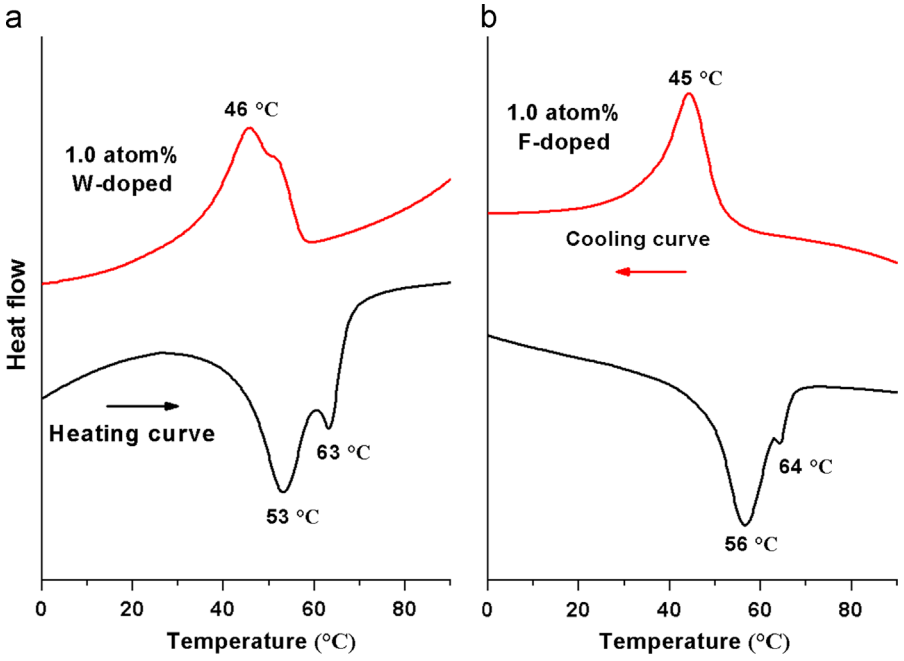

Fig. 15. DSC curves of W- and F-doped VO_2(M) prepared by the enlarged-scale experiments.

about 56 °C in the heating cycle and 45 °C in the cooling cycle, as depicted in Fig. 15.

4. Conclusion

(1) W-doped VO_2(M) was successfully synthesized via a hydrothermal reduction of V_2O_5 by $H_2C_2O_4$ in the presence of tungstic acid. Some parameters, such as the reaction temperature, reaction time, initial V_2O_5/oxalic acid molar ratio, tungstic acid concentration, were systematically investigated to reveal the formation of W-doped VO_2(M). The T_c of W-doped VO_2(M) can be simply tuned by changing the doping content of W atom when its concentration is less than 2.0 at%.

(2) The influence of different additives on the formation of VO_2 polymorphs by this facile hydrothermal route was studied. F, Ti, Cr, Fe, Mo, Sn, Sb and W atoms can promote the formation of VO_2(M), while Mg, Al, Co and Ni atoms are favorable for the synthesis of VO_2(B). Whereas, Na, Ca, Mn and Zn atoms have no influence on the formation of VO_2(A). The successful synthesis of VO_2 polymorphs can be attributed to the assistant function of the additives, which can affect the stabilization of the VO_6 octahedra in VO_2. W, Mo and F atoms can reduce the T_c of VO_2(M), whereas Ti, Cr, Fe, Sn and Sb atoms have little effect on the T_c.

(3) All of the as-obtained solid solutions of VO_2(M) have rod-like morphology in micro- and nano-scale.

(4) The variable-temperature infrared spectra show that the as-obtained doped VO_2(M) has outstanding thermochromic characters and optical switching properties, which can be used as the “smart window coating” and be beneficial

for the development and application of thermochromic materials.

(5) The enlarged-scale experiments for the preparation of doped VO_2(M) were carried out, and the similar results were obtained, the suggestive of its large-scale and low-cost synthesis, which can be used for potentially industrial production in future.

Acknowledgment

This work was partially supported by the Fundamental Research Funds for the Central Universities, the Youth Chenguang Project of Wuhan (201271031377), the Combination Project of Guangdong Province and the Ministry of Education (2011B090400397), and the Fundamental Research Funds for the Central Universities —Luojia Young Scholars Program (217273483).

Appendix A. Supporting information

Supplementary data associated with this article can be found in the online version at http://dx.doi.org/10.1016/j.ceramint.2013.04.016.

References

[1] X. Wang, J. Song, J. Liu, Z.L. Wang, Direct-current nanogenerator driven by ultrasonic waves, Science 316 (5821) (2007) 102–105.

[2] Y. Wu, J. Xiang, C. Yang, W. Lu, C.M. Lieber, Single-crystal metallic nanowires and metal/semiconductor nanowire heterostructures, Nature 430 (2004) 61–65.

[3] Y. Zhang, M. Fan, X. Liu, C. Huang, H. Li, Beltlike V_2O_3@C core–shell-structured composite: design, preparation, characterization, phase transition, and improvement of electrochemical properties of V_2O_3, European Journal of Inorganic Chemistry 2012 (10) (2012) 1650–1659.

[4] Y. Zhang, X. Liu, J. Nie, L. Yu, Y. Zhong, C. Huang, Improve the catalytic activity of α-Fe_2O_3 particles in decomposition of ammonium perchlorate by coating amorphous carbon on their surface, Journal of Solid State Chemistry 184 (2) (2011) 387–390.

[5] B.S. Guiton, Q. Gu, A.L. Prieto, M.S. Gudiksen, H. Park, Single-crystalline vanadium dioxide nanowires with rectangular cross sections, Journal of the American Chemical Society 127 (2) (2005) 498–499.

[6] P.X. Gao, Y. Ding, W. Mai, W.L. Hughes, C. Lao, Z.L. Wang, Conversion of zinc oxide nanobelts into superlattice-structured nanohelices, Science 309 (2005) 1700–1704.

[7] C. Lao, Y. Li, C.P. Wong, Z.L. Wang, Enhancing the electrical and optoelectronic performance of nanobelt devices by molecular surface functionalization, Nano Letters 7 (5) (2007) 1323–1328.

[8] Y. Zhang, X. Liu, G. Xie, L. Yu, S. Yi, M. Hu, C. Huang, Hydrothermal synthesis, characterization, formation mechanism and electrochemical property of $V_3O_7 \cdot H_2O$ single-crystal nanobelts, Materials Science and Engineering: B 175 (2) (2010) 164–171.

[9] Y. Zhang, J. Zhang, J. Nie, Y. Zhong, X. Liu, C. Huang, Facile synthesis of V_2O_3/C composite and the effect of V_2O_3 and V_2O_3/C on decomposition of ammonium perchlorate, Micro and Nano Letters 7 (8) (2012) 782–785.

[10] Y. Zhang, M. Fan, L. Hu, W. Wu, J. Zhang, X. Liu, Y. Zhong, C. Huang, Fabrication of V_2O_3/C core–shell structured composite and VC nanobelts by the thermal treatment of VO_2/C composite, Applied Surface Science 258 (24) (2012) 9660–9665.

[11] Y. Zhang, F. Zhang, L. Yu, M. Fan, Y. Zhong, X. Liu, Y. Mao, C. Huang, Synthesis and characterization of belt-like VO_2(B)@carbon and V_2O_3@carbon core–shell structured composites, Colloids and Surfaces A 396 (2012) 144–152.

[12] E. Strelcov, Y. Lilach, A. Kolmakov, Gas sensor based on metal–insulator transition in VO_2 nanowire thermistor, Nano Letters 9 (6) (2009) 2322–2326.

[13] Y.F. Zhang, X.H. Liu, D.Z. Chen, L. Yu, J.R. Nie, S.P. Yi, H.B. Li, C. Huang, Fabrication of $V_3O_7 \cdot H_2O$@C core–shell nanostructured composites and the effect of $V_3O_7 \cdot H_2O$ and $V_3O_7 \cdot H_2O$@C on decomposition of ammonium perchlorate, Journal of Alloys and Compounds 509 (5) (2011) L69–L73.

[14] I.P. Parkin, T.D. Manning, Intelligent thermochromic windows, Journal of Chemical Education 83 (3) (2006) 393–400.

[15] Y.F. Zhang, M. Zhou, M.J. Fan, C. Huang, C.X. Chen, Y.L. Cao, H.B. Li, X.H. Liu, Improvement of the electrochemical properties of $V_3O_7 \cdot H_2O$ nanobelts for Li battery application through synthesis of V_3O_7@C core–shell nanostructured composites, Current Applied Physics 11 (5) (2011) 1159–1163.

[16] H.S. Zhou, H.Q. Li, P. He, Y.G. Wang, E. Hosono, High-surface vanadium oxides with large capacities for lithium-ion batteries: from hydrated aerogel to nanocrystalline VO_2(B), V_6O_{13} and V_2O_5, Journal of Materials Chemistry 21 (29) (2011) 10999–11009.

[17] S. Milošević, I. Stojković, S. Kurko, J.G. Novaković, N. Cvjetićanin, The simple one-step solvothermal synthesis of nanostructurated VO_2(B), Ceramics International 38 (3) (2012) 2313–2317.

[18] Y. Zhang, C. Chen, W. Wu, F. Niu, X. Liu, Y. Zhong, Y. Cao, X. Liu, C. Huang, Facile hydrothermal synthesis of vanadium oxides nanobelts by ethanol reduction of peroxovanadium complexes, Ceramics International 39 (1) (2013) 129–141.

[19] K. Kim, S. Han Park, T. Hyung Kwon, H. Ahn, Y. Dam Eo, M.-J. Lee, Reaction sequence and electrochemical properties of lithium vanadium oxide cathode materials synthesized via a hydrothermal reaction, Ceramics International 39 (2) (2013) 1623–1629.

[20] Y. Zhang, C. Chen, J. Zhang, L. Hu, W. Wu, Y. Zhong, Y. Cao, X. Liu, C. Huang, Fabrication of belt-like VO_2(M)@C core–shell structured composite to improve the electrochemical properties of VO_2(M), Current Applied Physics 13 (1) (2013) 47–52.

[21] S. Milošević, Ž. Rašković-Lovre, S. Kurko, R. Vujasin, N. Cvjetićanin, L. Matović, J. Grbović Novaković, Influence of VO_2 nanostructured ceramics on hydrogen desorption properties from magnesium hydride, Ceramics International 39 (1) (2013) 51–56.

[22] W. Yu, J. Wang, Z. Gou, W. Zeng, W. Guo, L. Lin, Hydrothermal synthesis of vanadium pentoxide nanostructures and their morphology control, Ceramics International 39 (3) (2013) 2639–2643.

[23] Y. Zhang, J. Zhang, Y. Zhong, L. Yu, Y. Deng, C. Huang, X. Liu, Direct fabrication of organic carbon coated VO_2(B) (VO_2(B)@C) core–shell structured nanobelts by one step hydrothermal route and its formation mechanism, Applied Surface Science 263 (2012) 124–131.

[24] D. Hagrman, J. Zubieta, C.J. Warren, L.M. Meyer, M.M.J. Treacy, R.C. Haushalter, A new polymorph of VO_2 prepared by soft chemical methods, Journal of Solid State Chemistry 138 (1998) 178–182.

[25] B.Y. Qu, L. Liu, Y. Xie, B.C. Pan, Theoretical study of the new compound VO_2(D), Physics Letters A 375 (39) (2011) 3474–3477.

[26] J.A. Ni, W.T. Jiang, K. Yu, Y.F. Gao, Z.Q. Zhu, Hydrothermal synthesis of VO_2(B) nanostructures and application in aqueous Li-ion battery, Electrochimica Acta 56 (5) (2011) 2122–2126.

[27] Y. Zhang, M. Fan, M. Zhou, C. Huang, C. Chen, Y. Cao, G. Xie, H. Li, X. Liu, Controlled synthesis and electrochemical properties of vanadium oxides with different nanostructures, Bulletin of Materials Science 35 (3) (2012) 369–376.

[28] S. Zhang, B. Shang, J. Yang, W. Yan, S. Wei, Y. Xie, From VO_2(B) to VO_2(A) nanobelts: first hydrothermal transformation, spectroscopic study and first principles calculation, Physical Chemistry Chemical Physics 13 (2011) 15873–15881.

[29] Y. Zhang, Y. Huang, J. Zhang, W. Wu, F. Niu, Y. Zhong, X. Liu, X. Liu, C. Huang, Facile synthesis, phase transition, optical switching and oxidation resistance properties of belt-like VO_2(A) and VO_2(M) with a rectangular cross section, Materials Research Bulletin 47 (8) (2012) 1978–1986.

[30] Y. Zhang, M. Fan, X. Liu, G. Xie, H. Li, C. Huang, Synthesis of VO_2(A) nanobelts by the transformation of VO_2(B) under the hydrothermal treatment and its optical switching properties, Solid State Communications 152 (4) (2012) 253–256.
[31] Y. Zhang, M. Fan, F. Niu, Y. Zhong, C. Huang, X. Liu, B. Wang, H. Li, Hydrothermal synthesis of VO_2(A) nanobelts and their phase transition and optical switching properties, Micro and Nano Letters 6 (11) (2011) 888–891.
[32] F.J. Morin, Oxides which show a metal-to-insulator transition at the Neel temperature, Physical Review Letters 3 (1959) 34–36.
[33] A. Zylbersztejn, N.F. Mott, Metal–insulator transition in vanadium dioxide, Physical Review B 11 (11) (1975) 4383–4395.
[34] W. Burkhardt, T. Christmann, S. Franke, W. Kriegseis, D. Meister, B.K. Meyer, W. Niessner, D. Schalch, A. Scharmann, Tungsten and fluorine co-doping of VO_2 films, Thin Solid Films 402 (1–2) (2002) 226–231.
[35] J. Li, C.Y. Liu, L.J. Mao, The character of W-doped one-dimensional VO_2(M), Journal of Solid State Chemistry 182 (10) (2009) 2835–2839.
[36] L. Whittaker, T.L. Wu, C.J. Patridge, G. Sambandamurthy, S. Banerjee, Distinctive finite size effects on the phase diagram and metal–insulator transitions of tungsten-doped vanadium(IV) oxide, Journal of Materials Chemistry 21 (15) (2011) 5580–5592.
[37] C.X. Cao, Y.F. Gao, H.J. Luo, Pure single-crystal rutile vanadium dioxide powders: synthesis, mechanism and phase-transformation property, Journal of Physical Chemistry C 112 (48) (2008) 18810–18814.
[38] T.J. Hanlon, J.A. Coath, M.A. Richardson, Molybdenum-doped vanadium dioxide coatings on glass produced by the aqueous sol–gel method, Thin Solid Films 436 (2) (2003) 269–272.
[39] Y. Zhang, W. Li, M. Fan, F. Zhang, J. Zhang, X. Liu, H. Zhang, C. Huang, H. Li, Preparation of W- and Mo-doped VO_2(M) by ethanol reduction of peroxovanadium complexes and their phase transition and optical switching properties, Journal of Alloys and Compounds 544 (2012) 30–36.
[40] A.W. Smith, Optical storage in vanadium dioxide films, Applied Physics Letters 23 (8) (1973) 437–438.
[41] T.D. Manning, I.P. Parkin, M.E. Pemble, D. Sheel, D. Vernardou, Intelligent window coatings: atmospheric pressure chemical vapor deposition of tungsten-doped vanadium dioxide, Chemistry of Materials 16 (4) (2004) 744–749.
[42] S. Ji, F. Zhang, P. Jin, Preparation of high performance pure single phase VO_2 nanopowder by hydrothermally reducing the V_2O_5 gel, Solar Energy Materials and Solar Cells 95 (12) (2011) 3520–3526.
[43] Y. Zhang, M. Fan, F. Niu, W. Wu, C. Huang, X. Liu, H. Li, X. Liu, Belt-like VO_2(M) with a rectangular cross section: a new route to prepare, the phase transition and the optical switching properties, Current Applied Physics 12 (3) (2012) 875–879.
[44] C.G. Granqvist, Window coatings for the future, Thin Solid Films 193–194 (Part 2) (1990) 730–741.
[45] M.-H. Lee, J.-S. Cho, Better thermochromic glazing of windows with anti-reflection coating, Thin Solid Films 365 (1) (2000) 5–6.
[46] M.-H. Lee, Thermochromic glazing of windows with better luminous solar transmittance, Solar Energy Materials and Solar Cells 71 (4) (2002) 537–540.
[47] Z.F. Peng, Y. Wang, Y.Y. Du, D. Lu, D.Z. Sun, Phase transition and IR properties of tungsten-doped vanadium dioxide nanopowders, Journal of Alloys and Compounds 480 (2) (2009) 537–540.
[48] H. Wang, X. Yi, Y. Li, Fabrication of VO_2 films with low transition temperature for optical switching applications, Optics Communications 256 (4–6) (2005) 305–309.
[49] Y. Zhang, Y. Mao, D. Chen, W. Wu, S. Yi, S. Mo, C. Huang, Synthesis and characterization of addition-type silicone rubbers (ASR) using a novel cross linking agent PH prepared by vinyl-POSS and PMHS, Polymer Degradation and Stability 98 (4) (2013) 916–925.
[50] D. Chen, Y. Liu, C. Huang, Synergistic effect between POSS and fumed silica on thermal stabilities and mechanical properties of room temperature vulcanized (RTV) silicone rubbers, Polymer Degradation and Stability 97 (3) (2012) 308–315.
[51] S.A. Lawton, E.A. Theby, Effect of tungsten and molybdenum doping on the semiconductor–metallic transition in vanadium dioxide produced by evaporative decomposition of solutions and hydrogen reduction, Journal of the American Ceramic Society 78 (1) (1995) 238–240.
[52] Y. Zhang, M. Fan, W. Wu, L. Hu, J. Zhang, Y. Mao, C. Huang, X. Liu, A novel route to fabricate belt-like VO_2(M)@C core–shell structured composite and its phase transition properties, Materials Letters 71 (2012) 127–130.
[53] C.M. Zheng, X.M. Zhang, J.H. Zhang, K.R. Liao, Preparation and characterization of VO_2 nanopowders, Journal of Solid State Chemistry 156 (2) (2001) 274–280.
[54] Z.F. Peng, W. Jiang, H. Liu, Synthesis and electrical properties of tungsten-doped vanadium dioxide nanopowders by thermolysis, Journal of Physical Chemistry C 111 (3) (2007) 1119–1122.
[55] S. Yamamoto, N. Kasai, Y. Shimakawa, Preparation of monodisperse and spherical rutile VO_2 fine particles, Chemistry of Materials 21 (2) (2008) 198–200.
[56] J.Q. Shi, S.X. Zhou, B. You, L.M. Wu, Preparation and thermochromic property of tungsten-doped vanadium dioxide particles, Solar Energy Materials and Solar Cells 91 (19) (2007) 1856–1862.
[57] X. Liu, C. Huang, S. Yi, G. Xie, H. Li, Y. Luo, A new solvothermal method of preparing VO_2 nanosheets and petaloid clusters, Solid State Communications 144 (2007) 259–263.
[58] C.Z. Wu, J. Dai, X.D. Zhang, J.L. Yang, F. Qi, C. Gao, Y. Xie, Direct confined-space combustion forming monoclinic vanadium dioxides, Angewandte Chemie International Edition 49 (1) (2010) 134–137.
[59] J.H. Son, J. Wei, D. Cobden, G.Z. Cao, Y.N. Xia, Hydrothermal synthesis of monoclinic VO_2 micro- and nanocrystals in one step and their use in fabricating inverse opals, Chemistry of Materials 22 (10) (2010) 3043–3050.
[60] S.D. Ji, Y. Zhao, F. Zhang, P. Jin, Direct formation of single crystal VO_2(R) nanorods by one-step hydrothermal treatment, Journal of Crystal Growth 312 (2) (2010) 282–286.
[61] C.X. Cao, Y.F. Gao, L.T. Kang, H.J. Luo, Self-assembly and synthesis mechanism of vanadium dioxide hollow microspheres, CrystEngComm 12 (12) (2010) 4048–4051.
[62] F. Théobald, Étude hydrothermale du système VO_2–$VO_{2,5}$–H_2O, Journal of the Less Common Metals 53 (1) (1977) 55–71.
[63] Z. Gui, R. Fan, X.H. Chen, Y.C. Wu, A new metastable phase of needle-like nanocrystalline VO_2 center dot H_2O and phase transformation, Journal of Solid State Chemistry 157 (2) (2001) 250–254.
[64] Y. Zhang, J. Zhang, X. Zhang, C. Huang, Y. Zhong, Y. Deng, The additives W, Mo, Sn and Fe for promoting the formation of VO_2(M) and its optical switching properties, Materials Letters 92 (2013) 61–64.
[65] Y. Zhang, J. Zhang, X. Zhang, S. Mo, W. Wu, F. Niu, Y. Zhong, X. Liu, C. Huang, X. Liu, Direct preparation and formation mechanism of belt-like doped VO2(M) with rectangular cross sections by one-step hydrothermal route and their phase transition and optical switching propert ies, Journal of Alloys and Compounds 570 (2013) 104–113.
[66] F. Theobald, R. Cabala, J. Bernard, Essai sur la structure de VO_2(B), Journal of Solid State Chemistry 17 (4) (1976) 431–438.
[67] J.M. Longo, P. Kierkegaard, A refinement of the structure of VO_2, Acta Chemica Scandinavica 24 (1970) 420–428.
[68] S. Surnev, M.G. Ramsey, F.P. Netzer, Vanadium oxide surface studies, Progress in Surface Science 73 (4–8) (2003) 117–165.
[69] G. Silversmit, D. Depla, H. Poelman, G.B. Marin, R.D. Gryse, Determination of the V2p XPS binding energies for different vanadium oxidation states (V^{5+} to V^{0+}), Journal of Electron Spectroscopy and Related Phenomena 135 (2004) 167–175.
[70] C.D. Wagner, W.M. Riggs, L.E. Davis, J.F. Moulder, Handbook of X-Ray Photoelectrom Spectroscopy, Perkin-Elmer Corporation, Minnesota, 1979.
[71] C. Tang, P. Georgopoulos, M.E. Fine, J.B. Cohen, M. Nygren, G.S. Knapp, A. Aldred, Local atomic and electronic arrangements in $W_xV_{1-x}O_2$, Physical Review B 31 (2) (1985) 1000–1011.
[72] M. Tazawa, K. Yoshimura, K. Igarashi, S. Tanemura, K. Macák, U. Helmersson, Epitaxial growth of W-doped VO_2/V_2O_3 multilayer on

α-Al_2O_3(110) by reactive magnetron sputtering, Thin Solid Films 375 (1–2) (2000) 128–131.

[73] L. Whittaker, H. Zhang, S. Banerjee, VO_2 nanosheets exhibiting a well-defined metal–insulator phase transition, Journal of Materials Chemistry 19 (19) (2009) 2968–2974.

[74] S.A. Corr, M. Grossman, J.D. Furman, B.C. Melot, A.K. Cheetham, K.R. Heier, R. Seshadri, Controlled reduction of vanadium oxide nanoscrolls: crystal structure, morphology, and electrical properties, Chemistry of Materials 20 (20) (2008) 6396–6404.

[75] S.A. Corr, M. Grossman, Y.F. Shi, K.R. Heier, G.D. Stucky, R. Seshadri, VO_2(B) nanorods: solvothermal preparation, electrical properties, and conversion to rutile VO_2 and V_2O_3, Journal of Materials Chemistry 19 (25) (2009) 4362–4367.

[76] Y. Oka, T. Yao, N. Yamamoto, Structural phase transition of VO_2(B) to VO_2(A), Journal of Materials Chemistry 1 (5) (1991) 815–818.

[77] J. Galy, A proposal for (B) VO_2⇒(A) VO_2 phase transition: a simple crystallographic slip, Journal of Solid State Chemistry 148 (2) (1999) 224–228.

[78] C. Leroux, G. Nihoul, G. Van Tendeloo, From VO_2(B) to VO_2(R): theoretical structures of VO_2 polymorphs and in situ electron microscopy, Physical Review B 57 (9) (1998) 5111–5121.

[79] J.W. Ye, L. Zhou, F.J. Liu, J. Qi, W.T. Gong, Y.A. Lin, G.L. Ning, Preparation, characterization and properties of thermochromic tungsten-doped vanadium dioxide by thermal reduction and annealing, Journal of Alloys and Compounds 504 (2) (2010) 503–507.